Chapter 5

H_2 scattering from noble metal surfaces

5.1 Introduction: The H_2/metal system

The scattering or dissociation of gas phase (molecular beam) H_2 from/at transition metal surfaces, has served as a "drosophila" of gas surface dynamics in recent years. The system has a marked quantum behavior. H being the lightest among all atoms, both the vibrational and rotational energy levels of H_2 are clearly quantized. Very pronounced isotope effects are common, since the mass of H is one half of its isotope D. From a theorist's point of view, it is relatively easier to handle numerically because it has a small mass and only one electron. Last but not the least, it is of key importance in many chemical reactions, like Haber–Bosch ammonia synthesis or alkene hydrogenation. As a consequence, a large number of theoretical and experimental works were and are focused on this system.

From the theoretical point of view, the scattering and dissociation of H_2 as a quantum particle at rigid metals has been treated in the Born–Oppenheimer approximation with full dimensional Schrödinger equations, *i.e.*, with all six nuclear degrees of freedom of H_2 considered [137, 138, 139, 140, 141, 142]. Numerous other

high dimensional calculations are reviewed elsewhere [143, 144]. Moreover, there is a considerable number of experimental works that show the entangled dependence of the dynamics on all the dimensions of the system [145, 146, 147, 148]. This implies that it is essential to include as many degrees of freedom as possible in a simulation of a gas molecule encounter. On the other hand, both theory [16, 14] and experiments [149, 39, 40] show that the inclusion of the surface degrees of freedom is necessary for a complete description of the system, because even the full dimensional rigid surface calculations fail to have a quantitative agreement with the experimental results [141].

"Free" particle problems in gas phase dynamics, such as atom molecule scattering or photodissociation problems, as well as analogous problems in gas surface scattering or half–scattering, are frequently treated by using a coordinate grid onto which a nuclear wave function or a density matrix is mapped. Examples of these *collocation methods* are the Fourier grid method [127] (mostly used in connection with the Fast Fourier Transform algorithm), and the Discrete Variable Representation [150] (for both see Appendix A). In contrast, "bound" problems with not too many degrees of freedom, for which the corresponding (unperturbed) Hamiltonian can be diagonalized, are more economically handled within the eigenstate representation. On the other hand, the collocation methods have the advantage of being completely generally applicable.

In time dependent multi dimensional wave packet theory, the advantages of both representations have been combined by using simultaneously a grid for free, and a state representation for bound coordinates within the so called Coupled Channel Wave Packet (CCWP) method of Mowrey and Kouri [151, 152]. This expansion leads to coupled, low dimensional time dependent Schrödinger equations which are (if not too many bound functions are required) easier to solve than a single, higher dimensional one. So far, the CCWP method has been applied up to four and five dimensional molecule surface problems [153, 154, 155, 156].

When the surface cannot be considered as "rigid" (participation of phonons and/or electron hole pair excitations), and open system density matrix approach may be preferred over a Schrödinger dynamics. The numerical solution of Liouville–von

Neumann equations, however, is a considerably more time and memory consuming task than ordinary wave packet propagation, in particular for free problems. Kosloff and coworkers devised algorithms to solve dissipation free [71] or dissipative [81] Liouville–von Neumann equations *directly* (*i.e.*, by density matrix propagation), using a grid representation for all operators. Since the number of operations scales in this case with $N^2 \log N$ (rather than with $N \log N$ as for wave packet schemes) with the number of grid points, N, and since several *matrices* (rather than *vectors*) have simultaneously to be kept in central memory, this approach has so far been applied only to one dimensional examples (see [157, 158, 133], and chapter 4 for the case of photodesorption of NO from Pt).

In the following, we will consider the scattering of H_2 from a nonrigid metal surface. To account for experiments in which the H_2 bond was vibrationally excited [39], at minimum a two mode description for the "system" is required, but also the "bath" of substrate excitations must be accounted for. Hence we use a simple two dimensional molecule surface model, which historically played an important role in driving the analogous wave packet theory of diatom surface dynamics. In this model, which is the simplest one containing all the basic ingredients required to describe a surface molecule inelastic scattering, one only considers the coordinates Z (distance of the molecule's center of mass to the surface) and x (H_2 bond length) explicitly [159].

The dynamics is treated by a newly developed density matrix analog of the CCWP method, called the Coupled Channel Density Matrix (CCDM) method. This method is particularly well suited for the two dimensional, dissipative problem at hand, where motion along one coordinate (x) is bound, and motion along the other one (Z) free. Specifically, we consider H_2, D_2, and T_2 molecules inelastically scattering from a (nondissociative, nonreactive) noble metal model surface.

5.2 The Coupled Channel Density Matrix (CCDM) method

For the sake of simplicity, the CCDM equations are derived for the concrete example of inelastic scattering of a diatomic molecule from a surface. First, the equations of motion for the Hamiltonian (unitary) dynamics are introduced, because they are applicable to any two mode system. Then in section 5.5, the specific dissipation model is introduced, and the dissipative equations of motion are derived.

The two mode reduced dimensionality effective Hamiltonian $\hat{H}$ is[1]

$$\hat{H} = -\frac{1}{2\mu_x}\frac{\partial^2}{\partial x^2} - \frac{1}{2\mu_Z}\frac{\partial^2}{\partial Z^2} + V(x,Z) \quad . \tag{5.1}$$

In (5.1), x is the adsorbate interatomic distance, which is a bound coordinate at the energies of interest here (*i.e.*, the incoming molecule has a translational energy well below the activation energy for dissociation), and Z is (apart from a possible shift of the zero) the molecule surface distance, which is free at $Z \to +\infty$. μ_x and μ_Z are the corresponding reduced masses, *i.e.*, $\mu_x = m_H/2$ and $\mu_Z = 2m_H$, where m_H is the mass of an hydrogen atom. The molecule is assumed to approach the surface side on.

The classification of bound and free coordinates becomes clearer by introducing the model potential $V(x,Z)$ used. The mathematical form of this "elbow potential" $V(x,Z)$ is adopted from [160] and was originally designed for the system NO/Ag(111). We reparametrized it to resemble characteristic features found for the approach of H_2 to various sites of various copper surfaces. In particular, the model potential used in this subsection shows a "late" barrier to dissociation (at $x \approx 1.9\ a_0$ and $Z \approx 0\ a_0$), 0.6 eV high. The potential parameters (which have been changed) are given in Table 5.1.

The elbow potential is plotted in Fig.5.1 (the potential parameters for Fig.5.4 and in section 5.5 are different from the one used in here, because different systems are modeled). Next, we introduce a one dimensional *reference Hamiltonian* $\hat{H}_{ref}$,

[1] Here we drop the "$_s$" for $\hat{H}_s$ to avoid a too involved notation in the CCDM coupled equations.

Table 5.1: Computational parameters for (i) potential, (ii) density matrix propagation (for D_2, pure vibrational state $m = 0$, impact energy $\overline{E}_k(0) = 0.3$ eV), and (iii) bound state calculation for the reference Hamiltonian (see Eqn.(5.3)), for the model scattering of D_2 (H_2) from a Cu surface. The potential form is described in [160]. Here we give only those potential parameters, which are different from the ones given there.

Potential parameters			
	elbow potential		
		diatom Morse depth D	4.75 eV
		diatom Morse exponent	1.04436 a_0^{-1}
		diatom Morse equilibrium	1.40 a_0
	barrier		
		barrier location x	1.90 a_0
		barrier location Z	0.00 a_0
		x exponent β_x	5.00 a_0^{-1}
		Z exponent β_Z	2.50 a_0^{-1}
		barrier height	0.60 eV
	well		
		well depth	0.00 eV
Propagation parameters			
	grid parameters		
		grid spacing ΔZ	0.0945 a_0
		grid starting at	0.00 a_0
		grid ending at	12.00 a_0
		grid points N	128
	time propagation		
		timestep Δt	10 fs
		total propagation time t_∞	200 fs
		polynomial order n	170
	initial conditions		
		asymptotic reference Z_{ref}	8.0 a_0
		Gaussian width σ	1.00 a_0
Bound state calculations			
		grid starts at	0.8 a_0
		grid spacing Δx	0.031 a_0
		grid points N_x	50

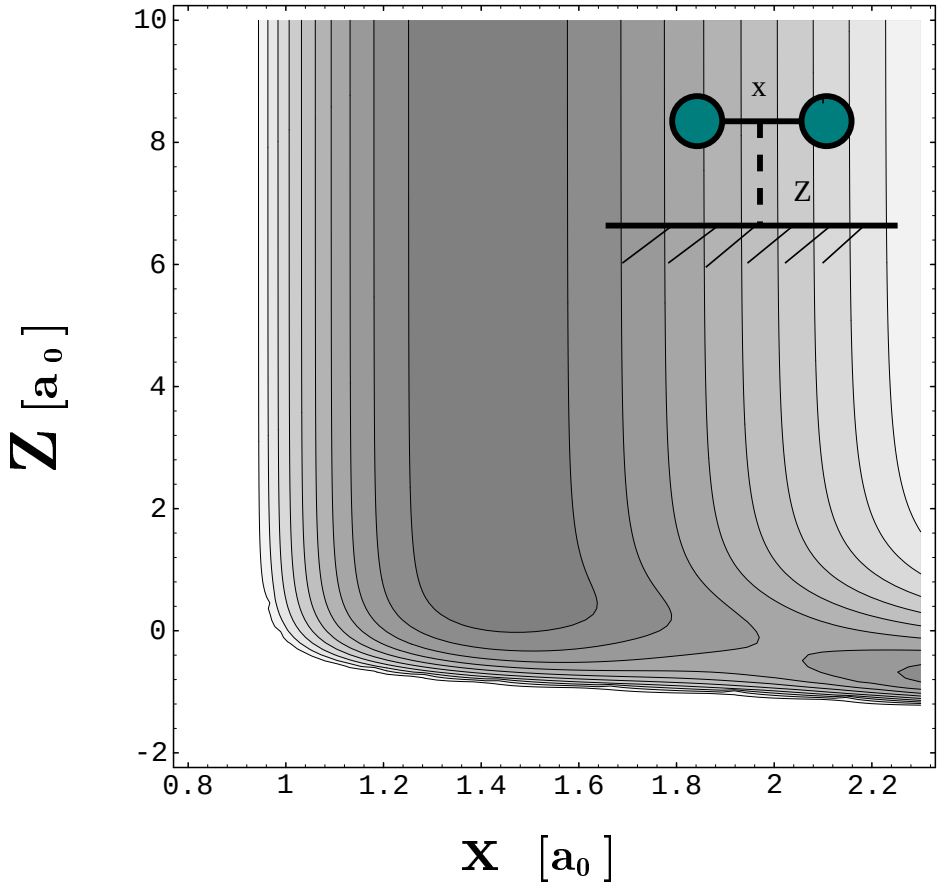

Figure 5.1: Contour plot of the model "elbow" potential $V(x, Z)$, adapted from Ref.[160] with the parameters indicated in table 5.1. This is the potential used in sections 5.2.-5.4. The contour spacing is 0.16 eV. The insert shows the definition of the bound (x) and free coordinate (Z), respectively.

$$\hat{H}_{ref} = -\frac{1}{2\mu_x}\frac{\partial^2}{\partial x^2} + V(x; Z_{ref}) \tag{5.2}$$

which governs the bound vibrational motion along x at a given value of the parameter Z_{ref}. The actual value to be chosen for Z_{ref} constitutes different possible reference Hamiltonians, and has a great influence on the numerical efficiency of the method (see below). Since one dimensional (in general: low dimensional) and bound in the

relevant energy range, $\hat{H}_{ref}$ can be easily diagonalized

$$\hat{H}_{ref}|m\rangle = \varepsilon_m|m\rangle \qquad , m = 0, 1, 2... \tag{5.3}$$

to give the reference eigenstates $|m\rangle$ and eigenenergies ε_m. Depending on the choice of Z_{ref} and the actual problem considered, the diagonalization can be done either analytically or numerically.

Using the reference eigenstates, we can spectrally decompose the density operator $\hat{\rho}$ as

$$\hat{\rho} = \sum_{m,m'=0}^{K-1} |m\rangle\langle m|\hat{\rho}|m'\rangle\langle m'| := \sum_{m,m'=0}^{K-1} \hat{\rho}_{mm'}|m\rangle\langle m'| \quad . \tag{5.4}$$

This expansion is exact, if the bound reference states form a complete set, and approximate, if a finite number of channels K is used. In this case, K is a convergence parameter. The expansion coefficients $\hat{\rho}_{mm'}$ are still operators in the subspace of the free coordinate(s).

We now

(i) use the expansion (5.4) in the Liouville–von Neumann equation (2.7), and

(ii) at the same time introduce a grid consisting of N points for the free coordinate.

Using further the notation[2]

$$A^{rs}_{mm'} := \langle r|\hat{A}_{mm'}|s\rangle := \langle r|\langle m|\hat{A}|m'\rangle|s\rangle$$

the time evolution of individual elements of the density matrix is

$$i\dot{\rho}^{rs}_{H,kl}(t) = \sum_{m=0}^{K-1}\sum_{t=1}^{N}(H^{rt}_{km}\rho^{ts}_{ml} - \rho^{rt}_{km}H^{ts}_{ml}) \quad . \tag{5.5}$$

[2]Lower indices denote k, l, m, m' bound states, upper indices r, s, t, u dissociative grid indices; integration over the respective independent variables.

where the index H denotes the Hamiltonian (dissipation free) case. Then, we rewrite the two dimensional Hamiltonian in (5.1) as

$$\hat{H} = \hat{H}_1 + \hat{H}_{ref} \tag{5.6}$$

$$\hat{H}_1 := -\frac{1}{2\mu_Z}\frac{\partial^2}{\partial Z^2} + V(x,Z) - V(x;Z_{ref}) \quad . \tag{5.7}$$

The individual matrix elements of $\hat{H}_{ref}$ and $\hat{H}_1$ are

$$H^{rt}_{ref,km} = \varepsilon_m \delta_{km}\delta_{rt} \tag{5.8}$$

$$H^{rt}_{1,km} = \delta_{km}T^{rt} + V^{tt}_{km}\delta_{rt} \quad . \tag{5.9}$$

In (5.8) and (5.9), δ_{ij} is the Kronecker delta[3]. Further, the following abbreviations have been used for the *free kinetic energy* and *channel coupling potential* matrix elements

$$T^{rt} := \langle r| - \frac{1}{2\mu_Z}\frac{\partial^2}{\partial Z^2}|t\rangle_Z \tag{5.10}$$

$$V^{tt}_{km} := \langle k|V(x,Z_t) - V(x,Z_{ref})|m\rangle_x \quad , \tag{5.11}$$

where $\langle \quad \rangle_y$ denotes integration over coordinate y. In deriving (5.8) and (5.9) we made use of the following relation

$$\langle r|f(Z)|s\rangle_Z = \delta_{rs} f(Z_s)$$

which holds both if a Fourier and a DVR grid is used ($f(Z)$ is a general function of Z).

Using (5.8) and (5.9) in (5.5) we get, element-wise, the *CCDM non–dissipative equations of motion*:

$$\begin{aligned} i\dot{\rho}^{rs}_{H,kl}(t) = (\mathcal{L}_H\hat{\rho})^{rs}_{kl} &= (\varepsilon_k - \varepsilon_l)\rho^{rs}_{kl} \\ &+ \textstyle\sum_{t=1}^{N}(T^{rt}\rho^{ts}_{kl} - \rho^{rt}_{kl}T^{ts}) \\ &+ \textstyle\sum_{m=0}^{K-1}(V^{rr}_{km}\rho^{rs}_{ml} - \rho^{rs}_{km}V^{ss}_{ml}) \quad . \end{aligned} \tag{5.12}$$

[3]Remember that the coordinates in standard quantum mechanics are a continuous index [1], but here we have performed a discretization [100, 127].

Apart from the grid indices, (5.12) constitutes a set of K^2 coupled one dimensional Liouville–von Neumann equations, or equivalently, a Liouville–von Neumann equation of block form. The first term on the r.h.s. of (5.12) describes rotation of the individual density matrix elements in the complex plane, without any coupling between them. The second term allows for the kinetic coupling between elements characterized by different grid indices, *i.e.* motion along the Z coordinate. The third term allows for the coupling between elements of different state indices, *i.e.*, vibrational transitions.

Note that if $K = 1$ ("vibrational adiabaticity"), Eqn.(5.12) reduces to

$$i\dot{\rho}^{rs} = [\hat{H}, \hat{\rho}]^{rs} \quad ,$$

which is (element-wise) simply a one dimensional Liouville–von Neumann equation along the free coordinate in grid representation. Similarly, for $N = 1$ ("coordinate adiabaticity"), Eqn.(5.12) reduces to

$$\begin{aligned} i\dot{\rho}_{kl} &= (\varepsilon_k - \varepsilon_l)\rho_{kl} + [V, \hat{\rho}]_{kl} \\ &= (\varepsilon_k - \varepsilon_l)\rho_{kl} \end{aligned} \tag{5.13}$$

because the coupling matrix elements V_{kl} are zero in this case. (5.13) is a (bound) Liouville–von Neumann equation in state representation. Hence, (5.12) satisfies the correct free and bound limits.

It is interesting to check how the algorithm behaves without dissipation, where it is easier to control the convergence and speed properties in comparison with normal wave packet simulations.

5.3 Numerical performance of the method

5.3.1 Numerical solution of the CCDM equations

The coupled equations (5.12) have to be solved numerically. This is done by the following steps.

1. *Time propagation.* The time propagation of the density operator was done by a Newtonian polynomial expansion of the time evolution superoperator (see section 3.2), with relations (3.21), (3.20), and (3.17).

2. *Kinetic coupling matrix elements for the free coordinate.* The kinetic energy matrix elements for the free coordinate, T^{rt} in (5.10), were calculated either by the FFT algorithm or the sinc–function DVR method (see Appendix A). The grid parameters (for the FFT case), which were usually used (unless otherwise specified), are also given in table 5.1[4].

3. *Potential coupling matrix elements for the bound coordinate.* To evaluate the potential coupling matrix elements V^{tt}_{km} defined in (5.11), we first have to evaluate the eigenfunctions of the one dimensional Hamiltonian $\hat{H}_{ref}$. This is done by using a sinc–function DVR grid [150] along the vibrational coordinate x (consisting of N_x points, say), and directly diagonalizing the resultant matrix $\mathbf{H_{ref}}$ to give N_x eigenfunctions $\langle x|m\rangle$ as vectors[5] $\mathbf{m}$. Eqn.(5.11) is then easily evaluated numerically because the coupling matrix $\mathbf{V}(Z_t)-\mathbf{V}(Z_{ref})$ is diagonal in coordinate space. The corresponding computational parameters are given in table 5.1.

5.3.2 Initial states

The solution of (5.12) requires the definition of an initial state, reproducing an experimental condition. Our goal is to model molecular beam experiments in which the incoming diatomic molecule has a Gaussian shape along Z, and is in
(i) either a *pure* or
(ii) a *thermal* state
with respect to its vibrational motion.

[4] Outside the grid boundaries, the potential is formally infinite and an energy cutoff is introduced. The eigenfunctions used in this work are defined for an energy cutoff of 2 eV, and with the grid parameters given in table 5.1. Different grid and cutoff parameters may lead to slightly different results; for the present methodologically oriented purposes this is not important, the results are converged for this choice of the potential.

[5] For this purpose the IMSL routine DEVESF 2.0 was used.

In the *pure state case* (vibrational state m), the individual density matrix elements at $t = 0$ are

$$\rho_{kl}^{rs}(0) = \langle r|\langle k|\hat{\rho}(0)|l\rangle_x|s\rangle_Z \tag{5.14}$$

$$\hat{\rho}(0) = g(Z)\cdot|m\rangle\langle m|\cdot g^*(Z') \implies \tag{5.15}$$

$$\rho_{kl}^{rs}(0) = g(Z_r)g^*(Z_s)\ \delta_{km}\delta_{ml} \quad , \tag{5.16}$$

where $g(Z)$ is the Gaussian of width σ centered far outside the surface at a point Z_∞, and approaching it along Z with mean momentum k_{0Z}:

$$g(Z) = \frac{1}{(\pi\sigma^2)^{1/4}} e^{-ik_{0Z}Z - \frac{(Z-Z_\infty)^2}{2\sigma^2}} \quad . \tag{5.17}$$

Similarly, in the case of a *thermal vibrational distribution* we start with a density of the form

$$\rho_{kl}^{rs}(0) = g(Z_r)g^*(Z_s)\cdot g_k\ \delta_{kl} \quad , \tag{5.18}$$

where g_k is the Boltzmann weight of state $|k\rangle$ at the vibrational gas temperature T_g, derived from

$$g_k = e^{-\varepsilon_k\beta} / \sum_m e^{-\varepsilon_m\beta} \quad . \tag{5.19}$$

In (5.19), $\beta := 1/k_bT_g$ has been used.

5.3.3 Scattering of D_2 from a Cu surface at $\overline{E}_k = 0.3$ eV

Benchmark calculations to test the performance of the CCDM method were carried out for D_2 scattering from the model Cu surface, when D_2 was in its vibrational ground state ($m = 0$ in (5.16)), and the average translational energy along Z, $\overline{E}_k(0) = k_{0z}^2/2\mu_Z$, was 0.3 eV. Further, the reference point Z_{ref} in (5.2) was asymptotically far away from the surface, $Z_{ref} = 8.0\ a_0$. In this case, the eigenstates of the reference Hamiltonian are just the Morse vibrational eigenstates of the free D_2 molecule. Fig.5.2 gives the population of the individual channels, $P_m(t)$,

$$P_m(t) = \mathrm{tr}\,(\hat{\rho}|m\rangle\langle m|) = \sum_r \rho_{mm}^{rr} \tag{5.20}$$

as a function of time. (The second equality in (5.20) follows immediately from the expansion (5.4) of the density operator). We note a significant population of the higher channels when the particle rebounces from the surface. It is further found

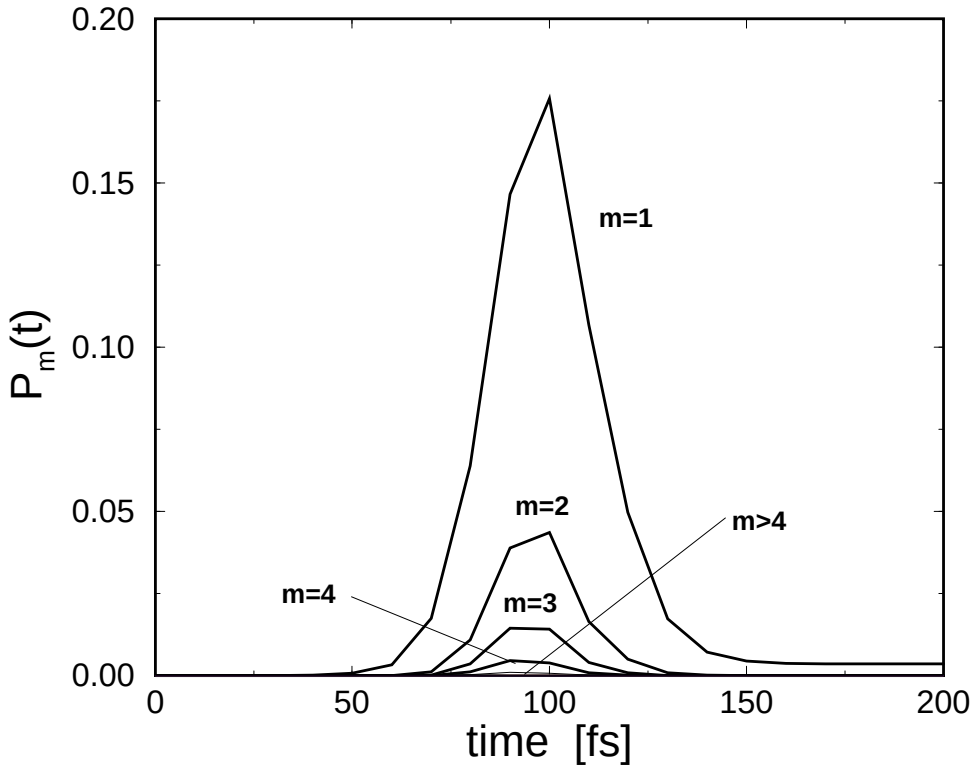

Figure 5.2: Channel populations $P_m(t)$ (Eqn.(5.20)), for D_2 ($m = 0$, $\overline{E}_k(0) = 0.3$ eV) scattering from the Cu model surface.

that for $t \to \infty$ (200 fs in practice), the D_2 molecule does not completely return into its vibrational ground state, but rather has gained a small population in the first excited state $m = 1$, $P_1(t_\infty = 200 \text{ fs}) = 0.00356$. (The $m = 0$ state is not shown in Fig.5.2 for clarity). Direct vibrational excitation of the type $m = 0 \to m = 1$ for H_2 and D_2 molecules rescattered from Cu(111) surfaces has also been observed experimentally [148, 161].

5.3.4 Convergence with respect to the number of channels

The calculation with $K = 12$ is rather expensive, both in terms of computation time and memory requirements. If no symmetry properties of the density matrix are used, there are $(12 \cdot 128) \times (12 \cdot 128) \approx 2.4 \cdot 10^6$ (complex) elements for a single density matrix, corresponding to a minimum memory requirement of 108 MBytes, if the Newton algorithm is used. Though $K = 12$ is already substantially less than what a two dimensional grid method would require, we are interested in the question of how many channels are actually needed to achieve convergence.

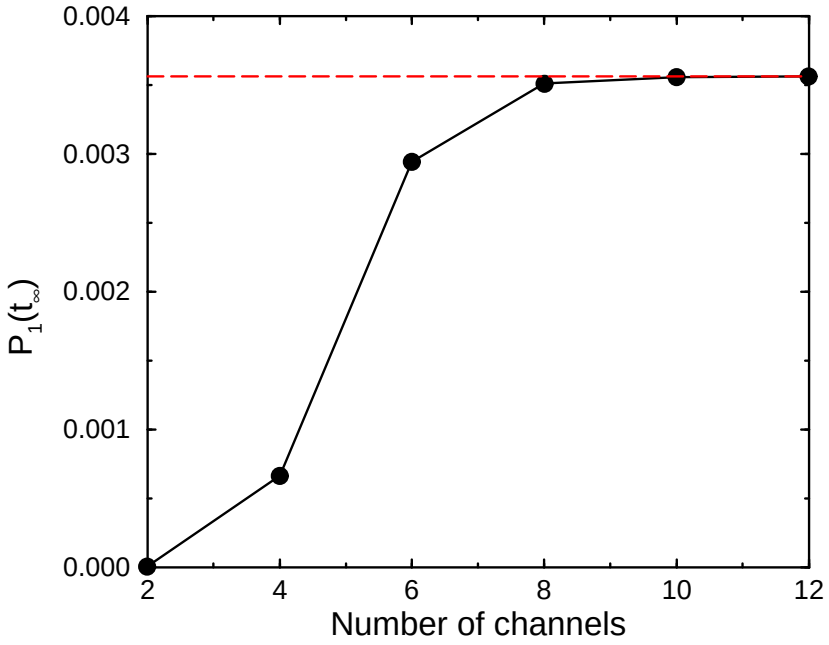

Figure 5.3: Convergence with respect to the number of channels, K, of the asymptotic first vibrational excited state population, $P_1(t_\infty)$, for D_2 ($m = 0$, $\overline{E}_k(0) = 0.3$ eV) scattering from the Cu model surface. The channel reference functions are for the asymptotic case, *i.e.*, $Z_{ref} = 8.0$ a_0. The circles are the CCDM results, while the dashed horizontal line gives the numerically converged result P_1^{ex}, obtained from a CCWP calculation with $K = 20$ (see text).

In Fig.5.3, for the same system and initial conditions as in the previous subsection, the convergence of $P_1(t = 200$ fs) as a function of K is investigated. It is found that already with $K = 8$, an accuracy of the fully converged ($K = 12$) result of $< 1.5\%$ is achieved. The corresponding computational effort, with regards to both memory and computation time is approximately 1/2 relative to the $K = 12$ case.

For the present, dissipation free situation numerically fully converged results can far more economically be obtained from wave packet theory, *i.e.*, from solving the time dependent Schrödinger equation. To make contact as close as possible with the

CCDM method, we used the coupled channel wave packet (CCWP) method alluded to earlier [151, 152], and employed exactly the same reference Hamiltonian $\hat{H}_{ref}$, and corresponding eigenfunctions $|m\rangle$ and eigenvalues ε_m as above. If $K = 12$ channels were included, the CCWP method gives a population P_1, which differs from the corresponding CCDM result by less than 0.002% ($P_1(t_\infty) = 3.56114 \cdot 10^{-3}$ (CCDM, $K = 12$), and $P_1(t_\infty) = 3.56119 \cdot 10^{-3}$ (CCWP, $K = 12$)). Further, by taking more and more channels into account in the CCWP calculation, we find that the results change from $K = 12$ to $K = 20$ by no more than 0.02% ($P_1(t_\infty) = 3.56194 \cdot 10^{-3}$ (CCWP, $K = 20$)). In the following, we will refer to the $P_1(t_\infty)$ (CCWP, $K = 20$) value as the "exact" population, P_1^{ex}. The numerically exact benchmark result P_1^{ex} is included in Fig.5.3 as a dashed horizontal line.

The question arises of how the accuracy of the CCDM method can be judged, if an exact or numerically converged benchmark is not available. Here, it is interesting to note that the maximum population of the highest channel considered ($K - 1$), gives a good estimate of the error made: It was found that this maximum population was approximately the same as the difference of the P_1 populations for the $K = 12$ case and the ones for $K < 12$. Hence, a reliable error estimate is possible by checking for the maximum population of P_{K-1} during the dynamic event.

5.3.5 Different reference Hamiltonians $\hat{H}_{ref}$

With reference to Fig.5.2, we note that the "bottleneck" of the calculation, with respect to the number of channels needed, is around $t = t_{coll} := 100$ fs, *i.e.*, when the D_2 is being reflected. This is understandable, since the basis used to represent the density matrix is optimized for a free molecule, so it's far from suited for a distorted molecule close to a surface, and requires a relatively large value of K. Indeed, again looking at Fig.5.2, for $t \ll t_{coll}$ a single basis function is sufficient (per definition), whereas for $t \gg t_{coll}$ more than one, but still not many channels are required.

Also the question arises, whether a different reference Hamiltonian leads, over the time, to a more uniform population of the individual channels, and if this helps

to reduce the maximum number of channels needed. Since we seek a basis better suited for the surface encounter, we choose as an alternative a reference Hamiltonian (5.2) with Z_{ref} close to the surface: $Z_{ref} = 0\ a_0$. We will call this choice henceforth the "surface reference" and the old one the "asymptotic reference". The resulting eigenfunctions, $|\tilde{m}\rangle$ of the surface reference Hamiltonian are no longer eigenfunctions of the free molecules and must be evaluated numerically.

Further, in practice, we will only use $\tilde{K}$ of those eigenfunctions, and hence the asymptotic eigenstates $|m\rangle$ can only be approximated by

$$|m\rangle \approx \sum_{\tilde{k}=0}^{\tilde{K}-1} |\tilde{k}\rangle C_{\tilde{k}m} \quad ,$$

where $C_{\tilde{k}m}$ is the scalar product $\langle\tilde{k}|m\rangle$.
This has the consequence of introducing an additional error when one is interested in the computation of populations defined in terms of the asymptotic states (*i.e.*, probabilities to find the free molecule in a particular vibrational state). These populations are easily found to be

$$P_m = \mathrm{tr}\left(\sum_{\tilde{k}=0}^{\tilde{K}-1}\sum_{\tilde{l}=0}^{\tilde{K}-1} \hat{\rho}_{\tilde{k}\tilde{l}} C_{\tilde{l}m} C^*_{\tilde{k}m}\right) \quad .$$

Numerically, it turns out for the present calculation (D_2, m=0, $\overline{E}_k(0) = 0.3$ eV), that with the choice $\tilde{K} = 6$, the additional relative error in computing P_m is estimated to be $< 10^{-5}$ ($m = 0$), $< 10^{-4}$ ($m = 1$) and $< 10^{-3}$ ($m = 2$). This estimate is based on the numerically obtained norms $\langle m|m\rangle$ of the asymptotic states, when expressed in the surface reference basis. Hence, for $m = 0$ and $m = 1$, the states which we are most interested in, the additional error is small for all practical purposes.

On the other hand, the benefit of using the new basis is given in table 5.2, where the relative errors in the time–asymptotic populations of the first excited vibrational level of D_2, $P_1(t = 200$ fs), are compared, as a function of the number of channels, for the asymptotic and the surface reference Hamiltonians $\hat{H}_{ref}$, respectively. The relative error was defined with respect to the numerically converged CCWP result

Table 5.2: Relative errors (5.21), (5.22) for the populations P_1 of channel $m = 1$ after inelastic scattering of D_2 molecules ($m = 0$, $\overline{E}_k(0) = 0.3$ eV) from the model Cu surface. The upper row is for the asymptotic reference ($Z_{ref} = 8.0$ a_0), the lower one for the surface reference ($Z_{ref} = 0.0$ a_0).

$K(\tilde{K})$	4	6	8	10	12
$E(K) \cdot 100\%$	81.47	17.46	1.46	0.14	0.02
$E(\tilde{K}) \cdot 100\%$	7.16	0.42	0.14	0.09	–

P_1^{ex} in the asymptotic basis, *i.e.*,

$$E(K) := \frac{|P_1(K) - P_1^{ex}|}{P_1^{ex}}, \tag{5.21}$$

$$E(\tilde{K}) := \frac{|P_1(\tilde{K}) - P_1^{ex}|}{P_1^{ex}}, \tag{5.22}$$

where the P_1 where for $t = 200$ fs. We find that, in comparison to the old one, with the new basis already with $\tilde{K} = 4$ an accuracy in the few percent regime can be achieved. Roughly, only half the number of channels is required with the new basis to arrive at a prespecified level of accuracy. This reduces the computational effort substantially – approximately by a factor of 4.

5.4 Inelastic molecule surface scattering

We now use the CCDM algorithm to study various different scattering experiments.

5.4.1 Different isotopomers and variation of impact energy

We first discuss effects associated with different particle masses and average translational energies. To this end, we consider H_2, D_2 and T_2 molecules in their vibrational

Table 5.3: The asymptotic first excited vibrational state population, $P_1(t_\infty)$, for H_2, D_2, and T_2 molecules (in their initial vibrational ground state) scattering from the Cu model surface, as a function of the initial average translational energy $\overline{E}_k(0)$.

$\overline{E}_k(0)$ [eV]	0.1	0.2	0.3	0.4
$P_1(t_\infty)(H_2)$	$< 10^{-5}$	$< 10^{-5}$	$5.40 \cdot 10^{-4}$	$1.06 \cdot 10^{-2}$
$P_1(t_\infty)(D_2)$	$< 10^{-5}$	$< 10^{-5}$	$3.56 \cdot 10^{-3}$	$9.35 \cdot 10^{-2}$
$P_1(t_\infty)(T_2)$	$< 10^{-5}$	$< 10^{-5}$	$3.93 \cdot 10^{-3}$	$1.56 \cdot 10^{-1}$

ground state, approaching the model Cu surface with various below–barrier average translational energies. In all cases we used the surface reference Hamiltonian ($Z_{ref} = 0\ a_0$), and $\tilde{K} = 6$ channel functions for H_2, $\tilde{K} = 8$ for D_2, and $\tilde{K} = 10$ for T_2 to account for the smaller vibrational level spacings for the heavier isotopomers. Also, we used different timesteps and total propagation times t_∞ (in the range between 150 and 425 fs) for the different impact energies, to account for the fact that faster molecules complete the scattering after a shorter time. For all isotopomers the same grid constant ΔZ given in table 5.1 turned out to be sufficient.

From table 5.3, which gives the population of the first vibrational state after the scattering was complete, $P_1(t_\infty)$, for the various isotopomers and impact energies, we see the following two trends:

(i) For a given average translational energy, $\overline{E}_k(0)$, the excitation probability increases with increasing mass of the isotopomer.

(ii) For a given isotopomer, the excitation probability increases with increasing average translational energy.

The first observation is a simple consequence of the fact that increasing reduced masses μ_x diminish the level spacings (and the zero point energy) for the asymptotic diatomic Morse oscillator. Therefore, excited states become easier accessible. The

second observation is due to the topology of the potential and can be explained along the lines drawn by Gates and Holloway [160] (for NO/Ag, though). Namely, the late barrier in Fig.5.1 allows high energy wave packets to probe the large curvature regions of the elbow potential, leading to a more efficient translation to vibration energy transfer.

5.4.2 Thermal initial states

The examples given so far could in principle also be obtained with single wave packet propagations, *i.e.*, by solving the time dependent Schrödinger equation. Next, we study effects associated with (vibrationally) thermal initial states of the type (5.18). In particular, we consider D_2 and T_2 with $\overline{E}_k(0) = 0.3$ eV, surface reference Hamiltonian with $\tilde{K} = 8$ (D_2) and $\tilde{K} = 10$ (T_2), and different gas temperatures T_g. The total propagation time was $t_\infty = 200$ fs ($\Delta t = 20$ fs, $n = 284$) for D_2, and $t_\infty = 300$ fs ($\Delta t = 25$ fs, polynomial order $n = 264$) for the heavier and slower T_2.

The propagation of thermal states can be done by a single propagation run in density matrix theory, whereas the Schrödinger equation would have to be solved for several wave packet runs. In the latter case, operator expectation values $\langle\hat{A}\rangle(t)$ are obtained by incoherent averaging over individual wave packet expectation values $\langle\hat{A}\rangle_m(t)$, where m is the index of the wave function m.

In table 5.4, we give the population of the individual channels (up to $m = 2$) prior and after the surface encounter ($t = 0$ and $t = t_\infty$, respectively), for all cases considered. The first columns, both for D_2 and T_2, are the $T_g = 0$ K results which partially have been given already in table 5.3, showing again that the surface scattering vibrationally excites the molecule. In table 5.4 (in brackets), we also give the ratio

$$R_m := \frac{P_m(t_\infty)}{P_m(0)} \tag{5.23}$$

of the pre and after scattering channel populations. If $R_m > 1$, a population gain of the corresponding channel took place relative to the initial state, whereas $R_m <$

Table 5.4: Channel populations prior to ($P_m(0)$) to and after ($P_m(t_\infty)$) inelastic scattering of D_2 (upper half) and T_2 (lower half) molecules ($m = 0$, $\overline{E}_k(0) = 0.3$ eV) from the model Cu surface. The numbers in brackets give the ratio R_m of the pre and after scattering probabilities (see Eqn.(5.23)).

D_2								
T_g [K]	0		600		900		1200	
$P_0(0)$	1		$9.99 \cdot 10^{-1}$		$9.92 \cdot 10^{-1}$		$9.74 \cdot 10^{-1}$	
$P_0(t_\infty)$	$9.96 \cdot 10^{-1}$	(0.996)	$9.96 \cdot 10^{-1}$	(0.997)	$9.91 \cdot 10^{-1}$	(0.999)	$9.78 \cdot 10^{-1}$	(1.009)
$P_1(0)$	0		$6.86 \cdot 10^{-4}$		$7.72 \cdot 10^{-3}$		$2.55 \cdot 10^{-2}$	
$P_1(t_\infty)$	$3.56 \cdot 10^{-3}$	(∞)	$3.81 \cdot 10^{-3}$	(5.555)	$8.63 \cdot 10^{-3}$	(1.118)	$2.08 \cdot 10^{-2}$	(0.816)
$P_2(0)$	0		$6.46 \cdot 10^{-7}$		$7.42 \cdot 10^{-5}$		$7.83 \cdot 10^{-4}$	
$P_2(t_\infty)$	$1.94 \cdot 10^{-5}$	(∞)	$2.27 \cdot 10^{-5}$	(35.139)	$1.35 \cdot 10^{-4}$	(1.819)	$8.67 \cdot 10^{-4}$	(1.107)
T_2								
T_g [K]	0		600		900		1200	
$P_0(0)$	1		$9.98 \cdot 10^{-1}$		$9.82 \cdot 10^{-1}$		$9.50 \cdot 10^{-1}$	
$P_0(t_\infty)$	$9.96 \cdot 10^{-1}$	(0.996)	$9.94 \cdot 10^{-1}$	(0.997)	$9.82 \cdot 10^{-1}$	(1.001)	$9.58 \cdot 10^{-1}$	(1.009)
$P_1(0)$	0		$2.48 \cdot 10^{-3}$		$1.80 \cdot 10^{-2}$		$4.74 \cdot 10^{-2}$	
$P_1(t_\infty)$	$3.76 \cdot 10^{-3}$	(∞)	$5.43 \cdot 10^{-3}$	(2.190)	$1.59 \cdot 10^{-2}$	(0.833)	$3.57 \cdot 10^{-2}$	(0.753)
$P_2(0)$	0		$7.64 \cdot 10^{-6}$		$3.81 \cdot 10^{-4}$		$2.63 \cdot 10^{-3}$	
$P_2(t_\infty)$	$4.09 \cdot 10^{-6}$	(∞)	$2.52 \cdot 10^{-4}$	(32.984)	$1.98 \cdot 10^{-3}$	(5.197)	$6.09 \cdot 10^{-3}$	(2.316)

1 indicates a depopulation. For $T_g = 0$ K, where the higher states are initially unpopulated, $R_m \to \infty$ for $m > 1$.

For a temperature of $T_g = 600$ K we note that the scattering leads again to vibrationally more excited products, for both isotopomers. The final state distribution is nonthermal – the logarithm of the individual channel populations is not any more a linear function of ε_m. Further, the excitation is more effective for the higher m.

By increasing the temperature even further, interesting observations are made.

(i) The absolute level of vibrational excitation increases.

(ii) The level of relative (to the initial state) vibrational excitation decreases with increasing T_g (for a given m, the R_m become smaller).

(iii) At the highest temperatures it may even happen that the first excited level $m = 1$, then already significantly populated at $t = 0$, is *depopulated* by the surface scattering event ($R_m < 1$).

In particular this last result is interesting in view of recent experiments by Gostein *et al.*, who observed substantial vibrational deexcitation of low energy $\overline{E}_k(0) = 0.078$ eV $H_2(m = 1)$ molecules scattered from a Cu(110) surface [39]. A more detailed discussion of this point will be given in section 5.5.

As a conclusion, the CCDM method allows for economical propagation of nuclear density matrices in more than one dimension, including free degrees of freedom. In particular, the memory problem is diminished by using a compact representation for the bound degrees of freedom. We have shown that a proper choice of the low dimensional bound reference Hamiltonian may lead to significant savings.

The next step is to add a dissipation mechanism to the equations of motion. An interesting test case are the recent scattering experiments done by Sitz and coworkers [39], for which we construct a physical model and compute properties to be compared to their empirical findings.

5.5 Dissipative dynamics with the CCDM method

5.5.1 The physical model

Here we will try to model the scattering of vibrationally excited H_2 and D_2 molecules approaching a cold, nonrigid and nondissociative surface. The term "nonrigid" is used here again in the sense that, when close enough, the molecule may excite phonons and electron hole pairs in the substrate and vibrationally relax. The electron hole pair mechanism is expected to be particularly efficient when the substrate is a metal [162]. In fact, an electronic mechanism has been suggested, for the experiment that we want to model, as one possible source for the experimentally observed 30% reduction of the $m = 1$ survival probability of slow H_2 ($m = 1$) molecules [initial kinetic energy $\overline{E}_k(0) = 78$ meV], inelastically scattered from a Cu(110) surface [39].

Electron hole pair excitation is also known to lead on a few ps time scale to the vibrational relaxation of adsorbed molecules [163, 164, 165], or to the trapping of gas phase atoms and molecules [162, 145, 7, 8, 166, 79]. Phonon creation leads to similar phenomena, but usually proceeds on significantly longer time scales. Temperature or radiation created phonons and electron hole pairs can further lead to the vibrational heating of adsorbates [167, 168] and even to their desorption [162, 169, 170] or predesorption [128, 129].

These dynamical processes can be categorized by the "system" plus "bath" concept and be described within open system density matrix theory. For our system, where a slow gas molecule is interacting with a bath of substrate electron hole pairs, the Markov approximation is expected to hold.

For dynamical gas surface encounters Redfield type approaches were also used to describe the sticking of rare gas atoms at copper model surfaces [166, 79], and the photodesorption of neutral molecules from metals [171]. For related work, see [172] and [173]. For the system we have to deal with, we preferred to use a Lindblad (2.11) form as Eqn.[55], as already mentioned in section 2.

Accordingly, we have chosen to construct a Markovian semigroup approach model and to derive the corresponding CCDM equations of motion for the "minimal" two mode model (unbound molecule surface coordinate Z, bound molecular bond coordinate x). A phenomenological relaxation model will be introduced. To cover from "weak" to "strong", and "short range" to "long range" dissipation a series of sensible parameters are considered. The dissipation model introduced below is expected to be suitable for a slow molecular beam of H_2 (D_2) ($m = 1$) molecules. For simplicity, we assume that the microscopic coupling of the impinging molecule to the (electron hole pairs of the) metallic substrate leads only to vibrational relaxation, while the center of mass motion remains unaffected. We further postulate a strong Z dependence of the vibrational relaxation rates. This is reasonable, because for $Z \to \infty$ a vibrational excited hydrogen molecule is stable on the time scales of interest, whereas vibrationally excited molecules adsorbed on metals relax typically within one to a few picoseconds [163, 164, 165]. The potential energy surface used in the following subsections is shown in Fig.5.4.

The barrier is again chosen to be "late", but insurmountably high[6] at least at the energies considered here. Hence, the molecule can at most be scattered inelastically from the surface, either due to translational to vibration (T–V) or V–T coupling, or due to energy exchange with the nonrigid surface. This is qualitatively the process expected to occur when gas phase hydrogen molecules interact with noble metal surfaces [175], and may be relevant for the experiments of Sitz and coworkers for the H_2/Cu(110) system [39].

The functional form of the potential is the same as for the nondissipative calculations (subsections 5.2-5.4), but it was adapted from [174]. The original potential was modified by removing the physisorption well, and shifting and increasing the barrier. The new potential parameters are given in table 5.5.

[6]We took a very high barrier (3.0 eV) to avoid dissociation of the molecule. In the case of dissociation the x mode becomes unbound, and then the CCDM approach must be modified.

Table 5.5: Computational parameters used for (i) the potential, (ii) the density matrix propagation, and (iii) the one dimensional bound state calculations [see Eqn.(5.3) and (5.32)]. The functional form of the potential is adapted from [174]. Here we give only those potential parameters which are different from those in [174]. The "typical" parameters for "grid and basis set" are for D_2 (m=1, $\overline{E}_k(0)$ = 78 meV) scattering from a nondissociative model surface; slightly different parameters have been used for other initial kinetic energies, or the other isotopomer. Similarly, the typical parameters for the "time propagation" depend on the actual dissipative parameters.

Potential parameters		
elbow potential		
	diatom Morse depth D	4.75 eV
	diatom Morse exponent	1.0280 a_0^{-1}
	diatom Morse equilibrium	1.40 a_0
barrier		
	barrier location x	2.6 a_0
	barrier location Z	0.8 a_0
	x exponent β_x	0.5 a_0^{-1}
	Z exponent β_Z	1.0 a_0^{-1}
	barrier height	3.0 eV
phys. well		
	well depth	0.00 eV
Propagation parameters		
grid and basis set parameters		
	typical grid starting at	0.00 a_0
	grid points N	128
	typical grid spacing ΔZ	0.11 a_0
number of channels K		10
time propagation		
	typical timestep Δt	10 fs
	typical polynomial order n	300
	total propagation time t_∞ (D_2)	460 fs ($\overline{E}_k(0)$ = 50 meV)
		390 fs ($\overline{E}_k(0)$ = 78 meV)
		340 fs ($\overline{E}_k(0)$ = 150 meV)
	total propagation time t_∞ (H_2)	290 fs ($\overline{E}_k(0)$ = 78 meV)
initial conditions		
	asymptotic reference Z_∞	8.0 a_0
	Gaussian width σ	0.5 a_0
Bound state calculations		
	grid starts at	0.4 a_0
	grid spacing along x, Δx	0.016 a_0
	grid points along x, N_x	250

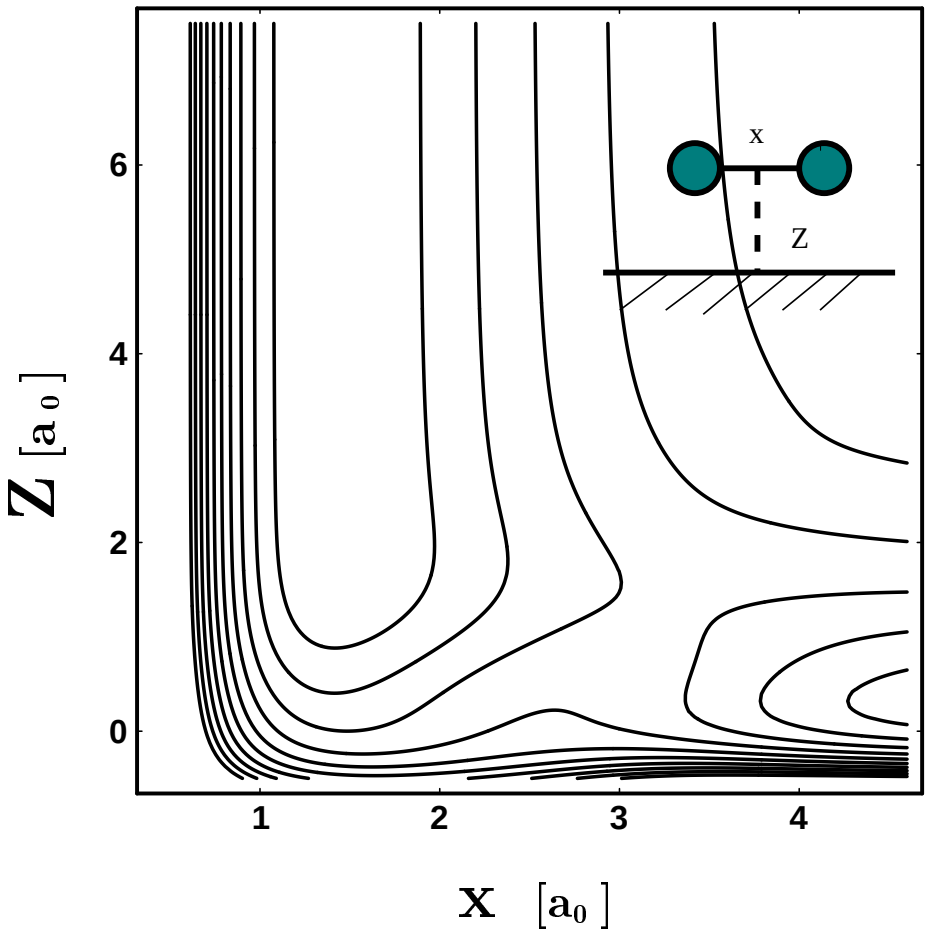

Figure 5.4: Contour plot of the model "elbow" potential $V(x, Z)$, adapted from Ref.[174] with the parameters indicated in table 5.5. This potential is used in section 5.5. The contour spacing is 1.0 eV. The insert shows the definition of the bound (x) and free coordinate (Z), respectively.

5.5.2 The CCDM dissipative equations of motion

Before deriving the dissipative CCDM equations of motion, we make some remarks about a more simple one dimensional system and derive for it the corresponding dissipation operators for the dissipative Liouville-von Neumann equation. This allows us to introduce the two dimensional model in a simpler fashion.

Consider an K dimensional discrete system Hilbert space. In order to describe an environment induced transition from level $|j\rangle$ to level $|i\rangle$ with a rate Γ_{ij}, it is convenient to choose for the Lindblad operator $\hat{C}_i$ in Eqn.(2.11) the following form [46, 43], with indices explicitly referring to the states connected by the operator :

$$\hat{C}_i \to \hat{C}_{ij} = \sqrt{\Gamma_{ij}}|i\rangle\langle j| \quad . \tag{5.24}$$

Here, we use positive elements Γ_{ij} for the relaxation matrix. For the diagonal elements we take $\Gamma_{ii} = 0$. Using (5.24) for the dissipative Lindblad operator (2.11) gives ($\rho_{ij} := \langle i|\hat{\rho}|j\rangle$):

$$\dot{\hat{\rho}}_D(t) = \sum_{ij=0}^{K-1} \Gamma_{ij} \left\{ |i\rangle\rho_{jj}\langle i| - \frac{1}{2}\left(|j\rangle\langle i|i\rangle\langle j|\hat{\rho} + \hat{\rho}|j\rangle\langle i|i\rangle\langle j|\right)\right\} \quad . \tag{5.25}$$

[We do not simplify Eqn.(5.25) for reasons which will become clear below.] Further, the corresponding $(K \times K)$ density and Hamiltonian operators are given by $\hat{\rho} = \sum_{ij=0}^{K-1} \rho_{ij}|i\rangle\langle j|$ and $\hat{H} = \sum_{ij=0}^{K-1} H_{ij}|i\rangle\langle j|$, respectively.

In general, the Hamiltonian in the basis of the *diabatic* functions $\{|i\rangle\}$ will not be diagonal. In fact, in the case of the (two dimensional) CCDM formalism of relevance here, the vibrational states are diabatically coupled [see Eqn. (5.12)]. In this case the diabatic energy curves along the free coordinate, Z, may cross. Then, an energy withdrawing "upper state $\to$ lower state" transition may become an unphysical process in which the system energy increases by turning into an "lower state $\to$ upper state" transition beyond the crossing point. More generally, problems arise when the offdiagonal elements of the Hamiltonian, H_{ij}, are nonzero.

These problems can be avoided by diagonalizing the system Hamiltonian and then defining the dissipation in the vibrationally *adiabatic* basis. However, we still treat the Hamiltonian evolution in the diabatic basis [see Eqn.(5.12)]. In the simple (one dimensional) K state case, let $\{|\alpha\rangle\}$ be the basis in which $\hat{H}$ is diagonal (Greek letters for the adiabatic basis). The new basis is related to the nondiagonal basis $\{|i\rangle\}$ (Roman letters for the diabatic basis) by

$$|\alpha\rangle = \sum_{i=0}^{K-1} |i\rangle S_{i\alpha} \quad , \tag{5.26}$$

where $S_{i\alpha} = \langle i|\alpha\rangle$ is a matrix element of the unitary transformation operator $\hat{S}$. Defining the dissipation adiabatically means to replace $\hat{C}_{ij}$ in (5.24) by $\hat{C}_{\alpha\beta}$, and to introduce transition rates $\Gamma_{\alpha\beta}$:

$$\dot{\hat{\rho}}_D(t) = \sum_{\alpha\beta=0}^{K-1} \Gamma_{\alpha\beta} \left\{ |\alpha\rangle\rho_{\beta\beta}\langle\alpha| - \frac{1}{2}\left(|\beta\rangle\langle\alpha|\alpha\rangle\langle\beta|\hat{\rho} + \hat{\rho}|\beta\rangle\langle\alpha|\alpha\rangle\langle\beta|\right)\right\} \quad . \tag{5.27}$$

To combine the dissipative part (5.27) with the Hamiltonian part which is still defined on the nondiagonal basis $\{|i\rangle\}$, we transform the dissipative part (5.27) to the diabatic basis (the "propagation basis"). The (k,l) matrix element of $\dot{\hat{\rho}}_D(t)$ in the propagation basis is

$$\dot{\rho}_{D,kl} = \sum_{\alpha\beta=0}^{K-1} \Gamma_{\alpha\beta} \left\{ \sum_{ij=0}^{K-1} S_{k\alpha}\ S_{\beta i}\ \rho_{ij}\ S_{j\beta}\ S_{\alpha l} \right. \tag{5.28}$$

$$\left. -\frac{1}{2}\sum_{ij=0}^{K-1} \left(S_{k\beta}\ S_{\alpha i}\ S_{i\alpha}\ S_{\beta j}\ \rho_{jl} + \rho_{ki}\ S_{i\beta}\ S_{\alpha j}\ S_{j\alpha}\ S_{\beta l}\right) \right\} \quad , \tag{5.29}$$

$$\tag{5.30}$$

where (5.26) and the orthonormality condition $\langle i|j\rangle = \delta_{ij}$ for the propagation basis functions have been used.

We now generalize to the two dimensional case with a bound motion represented again by K states, and a free motion along N grid points Z_r $(r = 1, 2, \ldots, N)$ (see subsection 5.2). For each coordinate point Z_r, we define

$$\hat{H}_r := -\frac{1}{2\mu_x}\frac{\partial^2}{\partial x^2} + V(x; Z_r) \quad , \tag{5.31}$$

and diagonalize,

$$\hat{H}_r|\alpha_r\rangle = \varepsilon_\alpha^r|\alpha_r\rangle, \alpha = 0, 1, 2, 3..., K-1. \tag{5.32}$$

Note that the propagation basis $\{|m\rangle\}$ of Eqn. (5.3) is $\{|m\rangle\} := \{|\alpha_{ref}\rangle\}$, where the subscript "ref" denotes the reference point Z_{ref} selected from the N grid indices.

In the spirit of the physical model discussed above, the general transition operators $\hat{C}_{ij}$ occurring in (2.11) are chosen such that no environment induced transitions

along the free coordinate Z are enforced. Further, transitions between the various bound states at each grid point Z_r shall be defined in the adiabatic basis $\{|\alpha_r\rangle\}$. We finally wish to allow for vibrational relaxation rates, which are coordinate dependent. To this end, we choose the following form for the operators of the Lindblad generator:

$$\hat{C}_{ij} \rightarrow \hat{C}_{\alpha\beta} = \sum_{r=1}^{N} \sqrt{\Gamma_{\alpha_c\beta_c} \cdot f(Z_r)}\ |r\alpha_r\rangle\langle\beta_r r| \quad . \tag{5.33}$$

Here, $\Gamma_{\alpha_c\beta_c} \geq 0$ is the transition rate connecting two (adiabatic) states at a second reference point, $Z = Z_c$. (In general, $Z_c \neq Z_{ref}$.) $f(Z)$ is a (positive) function accounting for the coordinate–dependence of the vibrational relaxation rates, and will be specified below.

We now insert the Lindblad operators (5.33) into Eqn.(2.11). Then we transform the dissipative generator to the propagation basis, and by using Eqn.(5.26) together with the orthonormality relations $\langle r|s\rangle_Z = \delta_{rs}$ and $\langle m|m'\rangle_x = \delta_{mm'}$ for the basis functions $\{|r\rangle\}$ in coordinate space, and the propagation functions $\{|m\rangle\}$, respectively, we arrive, element-wise, at

$$\begin{aligned} \dot{\rho}^{rs}_{D,kl} \;=\; & \textstyle\sum_{\alpha\beta=0}^{K-1} \sum_{ij=0}^{K-1} \Gamma_{\alpha_c\beta_c} \Big\{ \sqrt{f(Z_r)\ \cdot f(Z_s)}\ S_{k\alpha_r}\ S_{\beta_r i}\ \rho^{rs}_{ij}\ S_{j\beta_s}\ S_{\alpha_s l} \\ & -\tfrac{1}{2} \left(f(Z_r)\ S_{k\beta_r}\ S_{\alpha_r i}\ S_{i\alpha_r}\ S_{\beta_r j}\ \rho^{rs}_{jl} + f(Z_s)\ \rho^{rs}_{ki}\ S_{i\beta_s}\ S_{\alpha_s j}\ S_{j\alpha_s}\ S_{\beta_s l} \right) \Big\} \end{aligned} \tag{5.34}$$

where $S_{\alpha_s i}$, for example, stands for $\langle\alpha_s|i\rangle_x$. Note that in the case of a single grid point (Z_c, say), Eqn.(5.34) gives the correct one dimensional relation Eqn.(5.30).

At this point we stress that neither the use of the Lindblad generator (2.11), nor the choice (5.33) are unique; the suggested dissipative scheme is only one among several possible ones. The dissipative generator is Markovian, trace conserving, and leads to positive evolution. Further, no attempt is made at this stage to derive the parameters $\Gamma_{\alpha_c\beta_c}$ and the function $f(Z)$ from first principles.

In our CCDM approach, the Hamiltonian plus dissipative time evolution of the elements of the system density matrix is now given by

$$\dot{\rho}^{rs}_{kl} = \dot{\rho}^{rs}_{H,kl} + \dot{\rho}^{rs}_{D,kl} \quad , \tag{5.35}$$

with $\dot{\rho}^{rs}_{H,kl}$ and $\dot{\rho}^{rs}_{D,kl}$ defined in Eqn.(5.12) and (5.34), respectively. In practice, the number of channels, K, is used as a convergence parameter, and chosen as small as possible. This has the consequence that the completeness relation $\sum_j |j\rangle\langle j| = 1$ does not hold numerically, and therefore Eqn.(5.30) and (5.34) cannot be further simplified.

5.6 Numerical implementation

5.6.1 Time propagation

The time integration of the dissipative Liouville-von Neumann equation (2.9) is done again with the help of the Newton polynomial propagator as in the dissipation free case. The corresponding parameters are listed in table 5.5.

5.6.2 The operation $\mathcal{L}\hat{\rho}$

The evaluation of Eqn.(3.13) through (3.17) requires the knowledge of the action of the Liouvillian superoperator, $\mathcal{L}$ (as defined in Eqn.(2.9)), on the actual density operator, $\hat{\rho}(t)$, at every time t.

The Hamiltonian operation $\mathcal{L}_H\hat{\rho} = -i\left[\hat{H},\ \hat{\rho}\right]$ is performed as in section 5.3.1. The one dimensional bound Schrödinger equation (5.3) [and also (5.31)] was again solved by using the sinc–function discrete variable representation and diagonalizing the resulting Hamiltonian matrix as before. The reference point Z_{ref} was chosen as $Z_{ref} = 1.5\ a_0$. For the other parameters, see Table 5.5.

The dissipative operation $\mathcal{L}_D\hat{\rho}$ is more tricky. A brute force evaluation of Eqn. (5.34) scales as $O(K^6 \times N^2)$ with the number of channels, K, and the number of grid points, N. (Four sums over K indices for each element of the density matrix, the latter containing $K^2 \cdot N^2$ elements.) This scaling is prohibitive, even when K is not too

large. Fortunately, as shown in Appendix B, Eqn.(5.34) can be recast in a form which leads to a scaling of $O(K^3 \times N^2)$ which is much more favorable.

5.6.3 Computational parameters

The number of required channels, K, the number of grid points along Z, N, and the grid spacing along Z, ΔZ, were determined for the nondissipative case and are indicated in Table 5.5. Convergence tests were carried out for D_2 ($m = 1$) molecules, scattering from the model surface. Only pure state initial density matrices (see section 5.3.2) were considered, because of the experimental setup [39]. Here, $m = 1$ in (5.16) is the first excited eigenfunction of the free D_2 molecule, obtained by diagonalizing the 1D Hamiltonian $\hat{H}_r$ [Eqn.(5.31)] at the last grid point. The initial function along Z, $g(Z)$ in (5.16) is the same as in Eqn.(5.17). However, three kinetic energies were considered here, namely $\overline{E}_k(0) = 50$, 78, and 150 meV, respectively. The initial wave packet parameters σ and Z_∞, and typical basis set parameters K, N, and ΔZ, are listed in Table 5.5.

For analysis, the population of vibrational eigenstate $|m\rangle$ was obtained with Eqn.(5.20).

The grid and basis set parameters given in Table 5.5 were found to reproduce numerically "exact" populations P_0, P_1, P_2, and P_3 to within a relative error of less than 0.2%. (The "exact" values were obtained from benchmark calculations using the CCWP method.) The same parameters were used in the dissipative cases (see below); this – as made sure by numerical control experiments – did not introduce any significant additional error.

The total propagation time, t_{max}, was adjusted to allow for the complete reflection of the molecules within the time interval $[0, t_{max}]$, and is therefore dependent on the initial kinetic energies, and on the particular isotopomer studied . The typical Newton polynomial orders, n, and timesteps, Δt are given in Table 5.5.

5.7 Dynamics of D_2 (H_2) ($m = 1$) at nondissociative, cold metal surfaces

Calculations were carried out for both isotopomers H_2 and D_2 scattering from the nondissociative model surface. The molecules are initially in their first excited vibrational state [see Eqn. (5.16)], and approach the surface with mean translational energies $\overline{E}_k(0) \leq 150$ meV (see above).

5.7.1 Dissipative model and model parameters

Different dissipation parameters were used to cover a wide range of strengths and ranges for the relaxation. The function $f(Z)$ in (5.33) was assumed to be exponential,

$$f(Z) = \exp\{-\gamma(Z - Z_c)\} \quad , \tag{5.36}$$

where γ is a range parameter, and $Z_c = 0.5\ a_0$ is the distance between the $Z = 0$ plane and the minimum of $V(x, Z)$, which corresponds to dissociatively chemisorbed hydrogen atoms (the minimum for x larger than 4 a_0 in Fig.5.4). The exponential form derives from the fact that the electron hole pair mechanism here invoked must depend on the substrate electronic density, which decays to a good approximation exponentially with the distance from the surface plane. γ was varied between $\gamma = 2.5\ a_0^{-1}$ and $\gamma = 0.5\ a_0^{-1}$, corresponding to ranges of $R = 1/\gamma$ between 0.4 a_0 ("short range dissipation"), and 2.0 a_0 ("long range dissipation").

The dissipative model adopted for the relaxation matrix uses transition rates of the form

$$\Gamma_{\alpha_c\beta_c} = \begin{cases} \Gamma_{0_c1_c} \cdot \alpha \cdot \delta_{\alpha,\beta-1} & ,\beta > \alpha \\ 0 & ,\text{else.} \end{cases} \tag{5.37}$$

Here, the rates are given as multiples of a phenomenological transition rate $\Gamma_{0_c1_c}$, which is the rate for the decay of (adiabatic) level $|1_c\rangle$ to level $|0_c\rangle$, at $Z = Z_c$.

Eqn.(5.37) can be derived from a local polaron model for the coupling between substrate electron hole pairs and molecular vibrations, when perturbation theory to lowest order is used [168]. Eqn.(5.37) imposes "selection rules" by connecting only nearest neighbors along the vibrational ladder. Also, note that according to Eqn.(5.37) only "downward" transitions are possible. This is appropriate when the surface is cold, as assumed in the present model study.

For the dissipative strength parameter $\Gamma_{0_c 1_c}$, we took values between 1/50 fs^{-1} and 1/200 fs^{-1}. A hypothetical molecule ($m = 1$), permanently attached to the repulsive wall around $Z \approx Z_c$ of the potential given in Fig.5.4, would therefore vibrationally relax within "lifetimes" between $1/\Gamma_{0_c 1_c} = 50$ to 200 fs, respectively. The low energy molecules considered here, however, can only probe the significantly less repulsive regions of the potential. A molecule with initial kinetic energy $\overline{E}_k(0) =$ 78 meV, for example, has its classical turning point Z_{tp} at $Z_{tp} \approx 1.8$ a_0. As a crude estimate, therefore, a hypothetical molecule permanently attached to the classical turning point will vibrationally relax within

$$\tau \approx [\Gamma_{0_c 1_c} \cdot f(Z_{tp})]^{-1} \quad , \tag{5.38}$$

with $f(Z_{tp})$ given by Eqn.(5.36). In the present work, estimated lifetimes τ between 180 fs (for $\gamma = 1.0$ a_0^{-1}, $\Gamma_{0_c 1_c} = 1/50$ fs^{-1}, *i.e.*, "strong" dissipation of "long range") and $\approx$ 5.2 ps (for $\gamma = 2.5$ a_0^{-1}, $\Gamma_{0_c 1_c} = 1/200$ fs^{-1}, *i.e.*, "weak" dissipation of "short range") have been considered. Recalling that electron hole pair mediated vibrational relaxation of molecules adsorbed at metals typically takes place on a few ps time scale [163, 164, 165], the dissipative parameters adopted are of a realistic order of magnitude, provided the electron hole pair mechanism is assumed to be dominant. The question arises as to whether these lifetimes are short enough to account for a substantial reduction of the $m = 1$ survival probability during a scattering experiment for which the "contact time" between molecule and substrate is typically "short", of the order of 80, 100 and 130 fs for an average kinetic energy of 150, 78 and 50 meV, respectively

5.7.2 Dissipative *vs.* nondissipative scattering dynamics

In a first step, a dissipative scattering event was compared to the dissipation free case. For this purpose, D_2 ($m = 1$) molecules with an initial mean kinetic energy of $\overline{E}_k(0) = 78$ meV were scattered from the model surface, when the prefactor $\Gamma_{0_c1_c}$ in Eqn.(5.37) was $\Gamma_{0_c1_c} = 1/\infty \rightarrow 0$ (nondissipative or rigid surface case) and $\Gamma_{0_c1_c} = 1/100$ fs^{-1} (dissipative or nonrigid surface case), respectively. The dissipative range parameter was $\gamma = 1.5$ a$_0^{-1}$, leading, in the dissipative case, to a vibrational relaxation time at the classical turning point of $\tau \approx 0.7$ ps.

Fig.5.5a gives the asymptotic state populations $P_m(t)$, as defined in Eqn. (5.20). The solid curves refer to the dissipation free case, while the dashed ones are for the dissipative dynamics. In both cases P_0, P_2, and the summed populations $\sum_m P_m$ ($m \geq 3$) are shown, while P_1 is not given for clarity. (P_1 is 1 at $t = 0$, and remains > 0.9 at all times.) Let us consider the dissipation free case (solid curves) first. It is seen that with increasing time the populations of vibrational states other than $m = 1$ first increase, and then decrease again to almost zero. Maxima of the $P_m(t)$ curves emerge around $t \approx 150$ fs, when the molecule hits the surface. Though state $|1\rangle$ is still dominant, other states (in particular $|2\rangle$ and $|0\rangle$) come into play. For the propagation, $K = 10$ states was used (see Table 5.5), which gives well converged results. After $t_{max} \approx 390$ fs the scattering process is over. For the model potential used here (see Fig.5.4), at final time almost only *elastic* scattering is predicted at $\overline{E}_k(0) = 78$ meV – the population of the ground vibrational state at t_{max} is $P_0(t_{max}) < 10^{-4}$. Hence, the model potential allows for almost no V–T or T–V coupling, and a final ground state population $P_0(t_{max}) \neq 0$ can only arise when dissipation is present. Although our potential is not designed particularly for this system, we note that Sitz and coworkers observed for the $v = 0$ ground state of H_2 rescattered from Cu(110), a survival probability of 1.0 [39], indicative for weak T–V coupling also in that case.

As soon as dissipation is included, the situation changes (dashed lines in Fig.5.5). Now, at final time a significant fraction of the D_2 molecules (ca. 4%) has relaxed to the vibrational ground state. The final ground state population $P_0(t_{max})$ is a measure for the experimentally accessible survival probability of the $m = 1$ state,

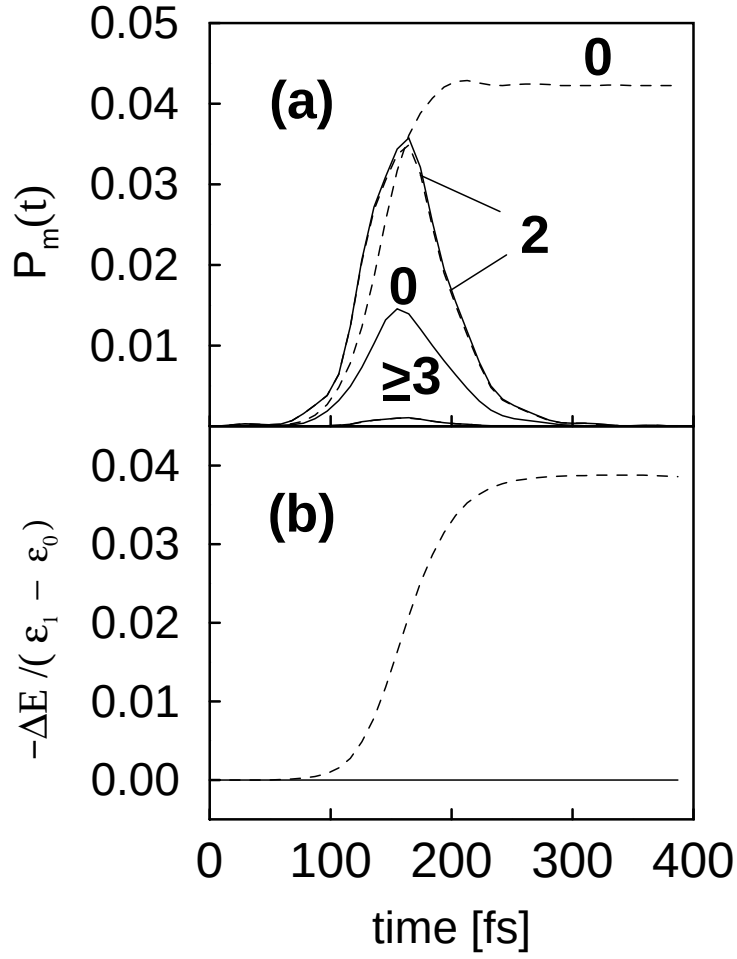

Figure 5.5: Scattering of D_2 ($m = 1$, $\overline{E}_k(0) = 78$ meV) from a nondissociative model surface: Comparison of dissipative (solid curves) with nondissipative dynamics (dashed curves). In the dissipative case, the strength parameter is $\Gamma_{0_c 1_c} = 1/100$ fs^{-1}, and the range parameter is $\gamma = 1.5$ a_0^{-1}. The meaning of these last parameters is given in section 5.7.1, Eqn.(5.36) and (5.37) . Panel (a) shows selected asymptotic state populations $P_m(t)$ [Eqn.(5.20)], while panel (b) gives the energy loss $\Delta E(t)$ [Eqn. (5.40)], in units of the fundamental vibrational quantum, $\varepsilon_1 - \varepsilon_0$, of free D_2.

i.e., $P_1(t_{max}) \approx 1 - P_0(t_{max})$, because under the present conditions no states other than $m = 0$ and $m = 1$ are populated when the scattering is over.

$P_0(t_{max})$ can roughly be estimated from the ratio of the time which the molecule spends close to the surface during scattering, t_{scat}, and the approximate lifetime of a hypothetical molecule localized close to the classical turning point, τ [see Eqn.(5.38)], multiplied by $1/e$. Hence,

$$P_0(t_{max}) \approx \frac{1}{e} \cdot \frac{t_{scat}}{\tau} \quad . \tag{5.39}$$

From Fig.5.5a we estimate $t_{scat} \approx 100$ fs, which gives $P_0(t_{max}) \approx \frac{1}{e} \cdot \frac{100\text{fs}}{0.7\text{ps}} \approx 0.05$, in close agreement with the observation.

It is further seen from Fig.5.5a that the $m = 2$ (and $m \geq 3$) populations are almost identical in the dissipative and nondissipative cases, respectively. This is because the dissipation was defined in the vibrationally *adiabatic* basis, rather than in the asymptotic basis $|m\rangle$, which is only used for analysis. The significant populations seen for the $m \geq 1$ states around $t \approx 150$ fs are therefore more due to the fact that the asymptotic basis is not well suited to mathematically represent the molecule when it strongly interacts with the surface, rather than due to "real" vibrational transitions. Vibrationally adiabatic states higher than $m = 1$ are never significantly populated, and therefore dissipation cannot influence them too much.

In Fig.5.5b, the energy loss of the system due to dissipation,

$$\Delta E(t) = \text{tr}\left(\hat{H}\left(\hat{\rho}(t) - \hat{\rho}(0)\right)\right) \quad , \tag{5.40}$$

is given for both cases studied in Fig.5.5a. We express ΔE in units of $\varepsilon_1 - \varepsilon_0$, *i.e.*, in units of the fundamental vibrational quantum of the free molecule. For the dissipation free case (solid) the system energy is conserved ($\Delta E = 0$), whereas in the dissipative case energy is transferred from the excited molecule to the surface. In our dissipative model the energy loss is only due to vibrational relaxation; $\Delta E(t_{max})$ must therefore be in the order of $P_0(t_{max}) \approx 0.04$, which is indeed the case.

Fig.5.5 demonstrates that an electron hole pair mechanism may account for vibrational relaxation in the few percent regime, when translationally slow D_2 ($m = 1$) molecules scatter from cold, nondissociative surfaces. The fraction of relaxed, scattered molecules can be estimated from Eqn.(5.39). In the following, we will address in some more detail how the fraction of relaxed molecules depends:

(i) on the dissipative model parameters,

(ii) on the kinetic energy of the incoming molecule, and

(iii) on isotopic substitution.

5.7.3 Variation of dissipative parameters

In Fig.5.6, the dependence of the survival probability of D_2 ($m = 1$) molecules on the dissipative *range parameter* γ is investigated for the case of $\overline{E}_k(0) = 78$ meV and $\Gamma_{0_c 1_c} = 1/100$ fs^{-1}. In Fig.5.6a, we give the population for the asymptotic vibrational ground state $|0\rangle$, $P_0(t)$ [Eqn.(5.20)], for five different range parameters ($\gamma = 0.5$, 1.0, 1.5, 2.0 and 2.5 a$_0^{-1}$, respectively). In Fig.5.6b the analogous information on the energy loss $\Delta E(t)$ [Eqn.(5.40)] is provided. It is seen that the longer the range of the dissipative forces, (*i.e.*, the smaller γ), the larger is the fraction of molecules which relax. At $t = t_{max}$ these fractions, *i.e.*, the populations $P_0(t_{max})$ are: 0.40 ($\gamma = 0.5$ a$_0^{-1}$), 0.12 ($\gamma = 1.0$ a$_0^{-1}$), 0.04 ($\gamma = 1.5$ a$_0^{-1}$), 0.017 ($\gamma = 2.0$ a$_0^{-1}$), and 0.006 ($\gamma = 2.5$ a$_0^{-1}$). The simple relation (5.39) gives, with $t_{scat} = 100$ fs, $P_0 = 0.19$, 0.10, 0.05, 0.02 and 0.01, respectively, and therefore accounts for the observed trend. The corresponding estimated vibrational relaxation times [(Eqn.5.38)] are $\tau \approx 200$ fs, 370 fs, 0.7 ps, 1.3 ps, and 2.6 ps, respectively.

From Fig.5.6b we note that the system energy is similar to Fig.5.5 – approximately given by the fraction of molecules relaxing to the vibrational ground state.

In Fig.5.7, the dependence of the results on the dissipative *strength parameter* $\Gamma_{0_c 1_c}$ is studied for D_2 ($m = 1$, $\overline{E}_k(0) = 78$ meV, $\gamma = 2.5$ a$_0^{-1}$). In Fig.5.7a the populations $P_0(t)$ are given, while Fig.5.7b shows once more the energy loss $\Delta E(t)$. The four different curves in each panel refer to $\Gamma_{0_c 1_c} = 1/50$ fs^{-1}, 1/100 fs^{-1}, 1/200 fs^{-1}, and $1/\infty$, respectively. From Eqn.(5.38) we estimate vibrational relaxation times of $\tau \approx 1.3$ ps, 2.6 ps, 5.2 ps, and ∞ for these cases. Fig.5.7 suggests that these "medium" to "weak" dissipative parameters lead to the vibrational relaxation of only small fractions of D_2 molecules. Both $P_0(t_{max})$ and $|\Delta E(t_{max})|$ do hardly exceed 0.01, even for the strongest coupling. To summarize, in particular from

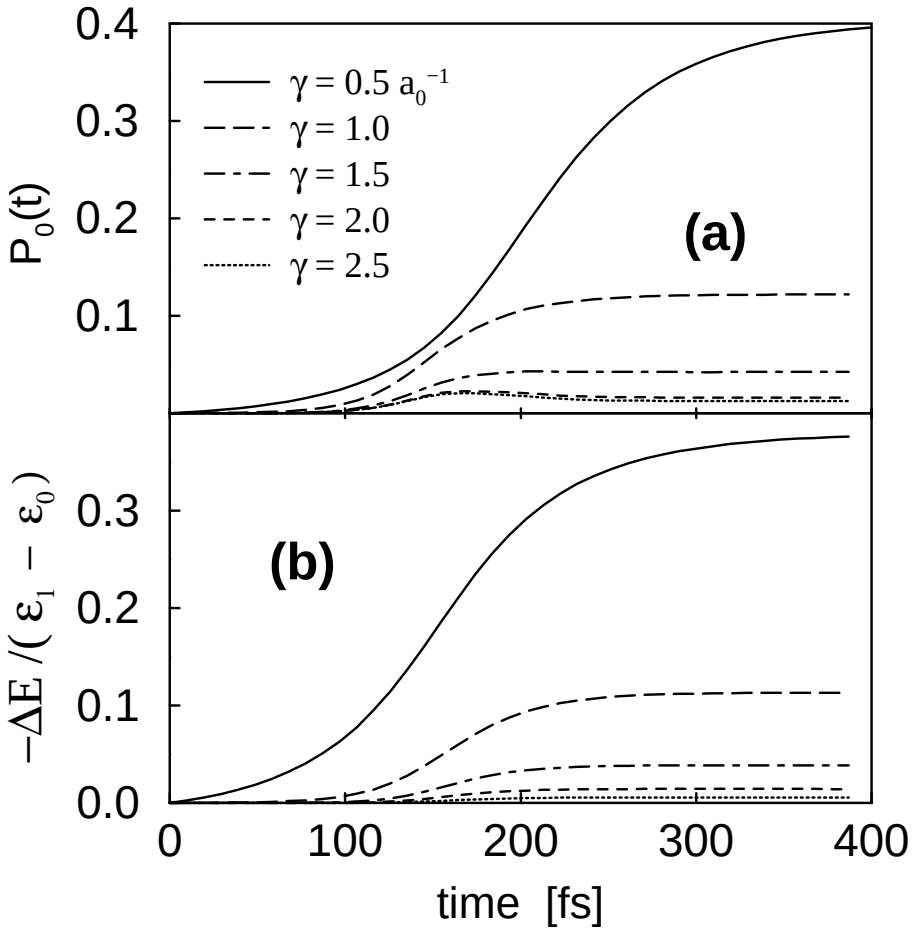

Figure 5.6: Scattering of D_2 ($m = 1$, $\overline{E}_k(0) = 78$ meV) from a model nondissociative surface: Comparison of different dissipative range parameters γ, at a fixed dissipative strength parameter, $\Gamma_{0_c 1_c} = 1/100$ fs^{-1}. The meaning of these last parameters is given in section 5.7.1, Eqn.(5.36) and (5.37) . Panel (a) shows the asymptotic ground state population $P_0(t)$ [Eqn. (5.20)], and panel (b) gives the system energy loss $\Delta E(t)$ [Eqn. (5.40)], in units of the fundamental vibrational quantum of free D_2.

Fig.5.6 it is concluded that the fraction of relaxed D_2 ($m = 1$) molecules can in principle cover the range seen by the experiment on the H_2 ($m = 1$) / Cu(110) system [39], which is in the order of 0.3. However, it must be stressed that this is only true when the dissipation is very "long range", and / or "strong", and the corresponding

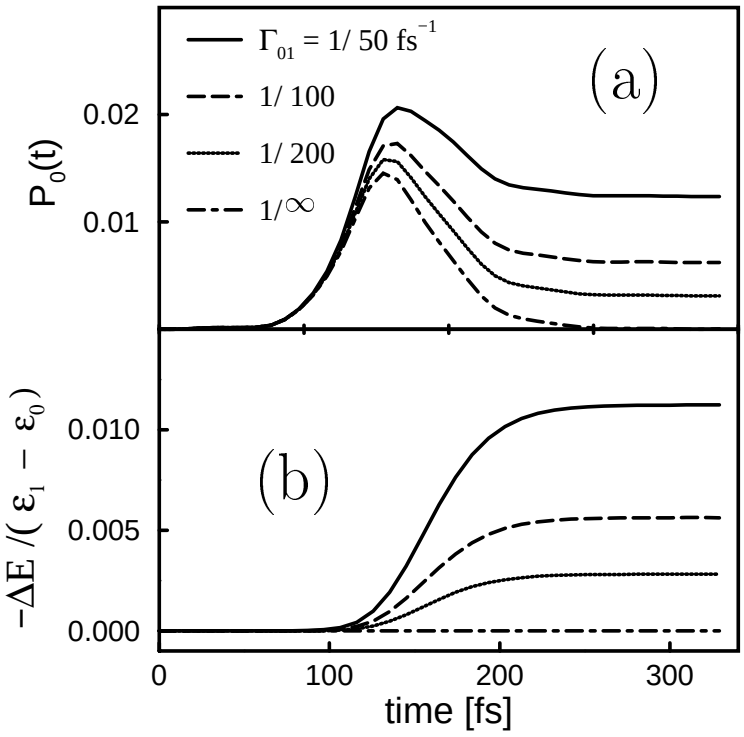

Figure 5.7: Scattering of D_2 ($m = 1$, $\overline{E}_k(0) = 78$ meV) from a model nondissociative surface: Comparison of different dissipative strength parameters $\Gamma_{0_c 1_c}$, at a fixed dissipative range parameter, $\gamma = 2.5$ a_0^{-1}. The meaning of these last parameters is given in section 5.7.1, Eqn.(5.36) and (5.37) . Panels (a) and (b) give information analogous to Fig.5.6.

vibrational relaxation times sufficiently (probably unrealistically), short.

This is in more detail demonstrated in Fig.5.8, where computed final ground state populations $P_0(t_{max})$ are shown as a function of the approximate vibrational relaxation time τ [Eqn.(5.38)]. By varying the dissipative parameters γ and $\Gamma_{0_c 1_c}$, a lifetime range between 180 fs and 5.2 ps was covered. The calculations refer to D_2 ($m = 1$, $\overline{E}_k = 78$ meV). The symbols shown in Fig.5.8 are the numerical values obtained with the CCDM method. The dashed curve is an estimate for $P_0(t_{max})$, resulting from the simple relation (5.39), when $t_{scat} = 100$ fs is used. Note that the numerically "exact" populations follow closely the simple $1/\tau$ behavior predicted by Eqn. (5.39). Both from the numerically exact and the approximate data, it can

be argued that the experimental 30% reduction of the $m = 1$ population for H_2 / Cu(110) [39] requires a vibrational relaxation time of 200 fs or so. This seems too short (by a factor of ≈ 10) to be realistic, for a closed shell molecule relaxing *via* an electron hole mechanism at a metallic substrate [163, 164, 165]. Though differences between H_2 and D_2 molecules are to be expected (see below), and though our model and the potential used are not necessarily representative for H_2/Cu(110), we conclude that electron hole pair excitation alone can hardly account for the experimentally observed reduced survival probability of H_2 ($m = 1$) at Cu(110) [39]. However, the reduction of the $m = 1$ population by a few percent seems possible, when realistic vibrational lifetimes τ are assumed.

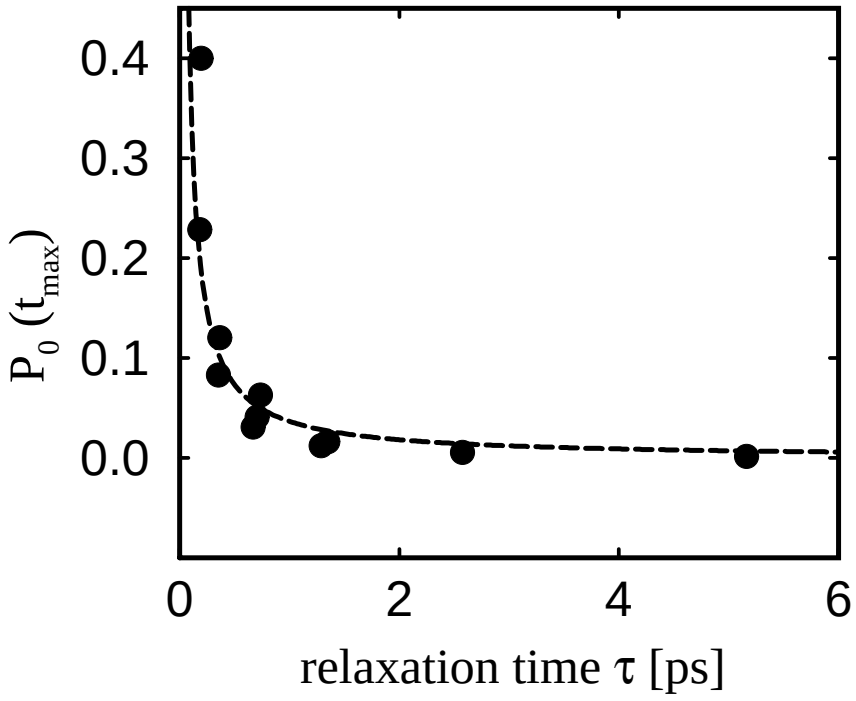

Figure 5.8: Scattering of D_2 ($m = 1$, $\overline{E}_k(0) = 78$ meV) from a model nondissociative surface: Final vibrational ground state population $P_0(t_{max})$, as a function of the estimated vibrational relaxation time at the classical turning point, τ [Eqn. (5.38)]. The symbols are the results of the CCDM approach, while the dashed curve arise from the simple, approximate relation (5.39) with the choice $t_{scat} = 100$ fs.

5.7.4 Variation of initial mean kinetic energies

In a further step, the dependence of the inelastic scattering process on the initial mean kinetic energy $\overline{E}_k(0)$ of the incoming molecule was studied. For this purpose, calculations for D_2 ($m = 1$) with $\overline{E}_k(0) = 50$, 78, and 150 meV were carried out. The dissipative strength parameter was $\Gamma_{0_c 1_c} = 1/100$ fs^{-1}, while two different range parameters γ ($\gamma = 2.5$ and $\gamma = 1.5$ a$_0^{-1}$) were used.

In Fig.5.9a, the vibrational ground state population $P_0(t)$ is shown for all six cases studied (two range parameters, three kinetic energies), while Fig.5.9b gives the analogous information for the system energy loss, $\Delta E(t)$. From Fig.5.9b, for example, we note that our simple model predicts the following. The larger the $\overline{E}_k(0)$, the earlier the molecule hits the surface, and the earlier the loss of energy sets in. Further, the transition region connecting the two plateau regions at short and long times t, is the steeper the larger $\overline{E}_k(0)$. The final energy transfer $\Delta E(t_{max})$ to the substrate is largely independent of the initial kinetic energy. This observation holds for different range parameters γ. Analogous conclusions are drawn from the population curves given in Fig.5.9a.

The explanation of this remarkable insensitivity of the vibrational relaxation process on initial kinetic energy is easily explained with the help of the approximate relation (5.39). The higher the $\overline{E}_k(0)$, the closer to the surface is the classical turning point; via Eqn.(5.38) and Eqn.(5.36), this implies a shorter vibrational relaxation time, τ. According to Eqn.(5.39), this leads to an *increase* of the asymptotic state population, $P_0(t_{max})$. However, the faster the molecule the shorter the interaction time t_{scat}, which leads, again *via* (5.39), to a *decreased* relaxation probability. Both effects largely compensate, giving rise to the observed insensitivity of the final properties on $\overline{E}_k(0)$.

5.7.5 Isotope effects

In a final series of calculations, effects of isotopic substitution were studied by contrasting D_2 ($m = 1$) scattering with H_2 ($m = 1$) scattering. For fixed $\overline{E}_k(0) = 78$

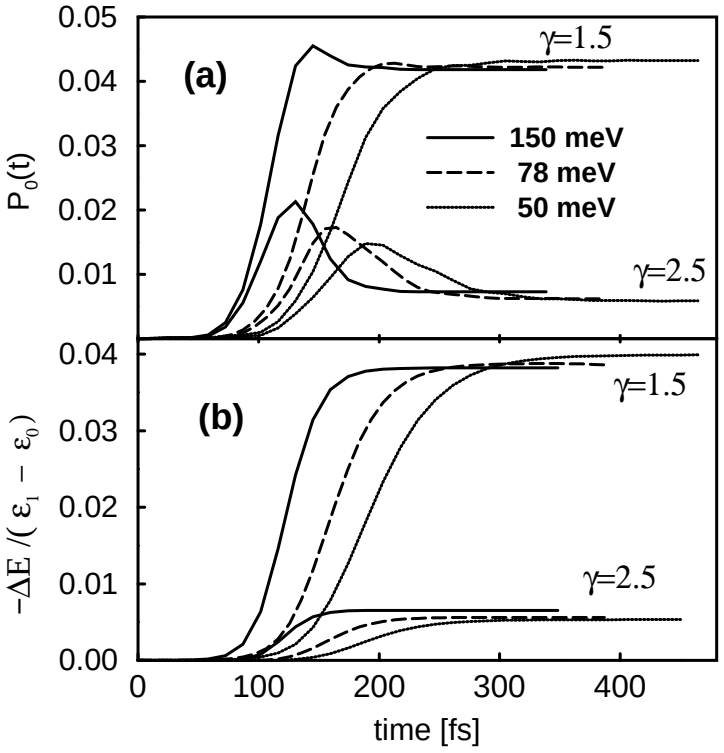

Figure 5.9: Scattering of D_2 ($m = 1$) from a model nondissociative surface: Comparison of different mean initial kinetic energies, $\overline{E}_k(0)$. Three kinetic energies $\overline{E}_k(0) = 50$, 78, and 150 meV and two different dissipative range parameters $\gamma = 1.5$ a_0^{-1} and $\gamma = 2.5$ a_0^{-1}, are considered. The dissipative strength parameter is fixed at $\Gamma_{0_c 1_c} = 1/100$ fs^{-1}. The meaning of the dissipation parameters is given in section 5.7.1, Eqn.(5.36) and (5.37) . Panels (a) and (b) give information analogous to Fig.5.6.

meV, and at a fixed dissipative strength parameter ($\Gamma_{0_c 1_c} = 1/100$ fs^{-1}), different dissipative range parameters were considered ($\gamma = 1.0$, 1.5, and 2.0 a_0^{-1}, respectively). A comparison between both isotopomers is given in Fig.5.10, where again vibrational ground state populations (Fig.5.10a) and energy losses (Fig.5.10b) are shown. From Fig.5.10a we note that the vibrational relaxation is more efficient in the case of D_2, but the differences are not huge. For instance, with $\gamma = 1.0$ a_0^{-1}, $P_0(t_{max})$ is 0.088 for H_2, and $P_0(t_{max}) = 0.12$ for D_2. For $\gamma = 2.0$ a_0^{-1}, the corresponding numbers are 0.012 (H_2), and 0.017 (D_2), respectively.

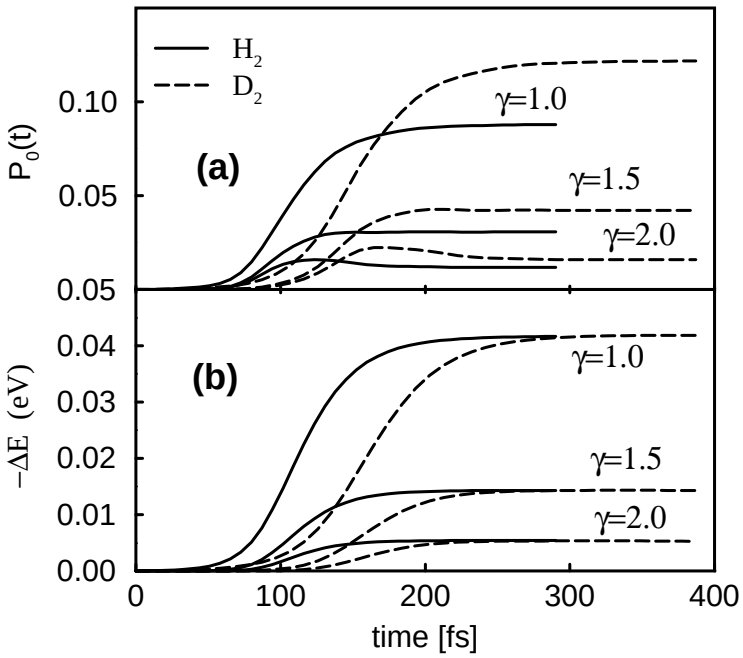

Figure 5.10: Comparison of H_2 ($m = 1$, $\overline{E}_k(0) = 78$ meV) with D_2 ($m = 1$, $\overline{E}_k(0) = 78$ meV) for the scattering from a model nondissociative surface. Three different dissipative range parameters γ are considered, at a fixed dissipative range parameter, $\Gamma_{0_c 1_c} = 1/100$ fs^{-1}. The meaning of the parameters is given in section 5.7.1. Panels (a) and (b) give the information analogous to Fig.5.6, except that in (b) absolute energy units have been used.

Hence, the ratio $P_0(t_{max})(H_2)/P_0(t_{max})(D_2)$ is remarkably close to $\sqrt{2}$, which is the ratio of the classical velocities of H_2 and D_2 when approaching the surface with the same kinetic energy $\overline{E}_k(0)$. The simple classical model (5.39) can also account for the observed isotope effect. Namely, due to the higher velocity of the lighter isotopomer, the H_2 scattering time t_{scat} will be shorter by a factor of about $\sqrt{2}$. Since the classical turning points, and hence the estimated vibrational relaxation times τ are the same for both isotopomers, Eqn. (5.39) explains the higher survival probability for $H_2(m = 1)$.

The final energy loss $\Delta E(t_{max})$, which is given in Fig.5.10b, is approximately

the same for both isotopomers if absolute energy units are used. This is because of the cancellation of two effects. The H_2 molecule loses about a factor of $\sqrt{2}$ less vibrational quanta than D_2, but the absolute energy of the H_2 fundamental vibrational quantum is by a factor of about $\sqrt{2}$ larger than that of D_2. The observed isotope effects rely on the approximation that the dissipative parameters are the same for both isotopomers.